AMERICAN SOCIETY FOR MICROBIOLOGY | Infection and Immunity

Host-Microbial Interactions | Full-Length Text

Contribution of bacterial and host factors to pathogen "blooming" in a gnotobiotic mouse model for *Salmonella enterica* serovar Typhimurium-induced enterocolitis

Markus Beutler,[1] Claudia Eberl,[1] Debora Garzetti,[1] Simone Herp,[1] Philipp Münch,[1,2,3] Diana Ring,[1] Tamas Dolowschiak,[4,5] Sandrine Brugiroux,[1] Patrick Schiller,[1] Saib Hussain,[1] Marijana Basic,[6] André Bleich,[6] Bärbel Stecher[1,7]

AUTHOR AFFILIATIONS See affiliation list on p. 15.

ABSTRACT Inflammation has a pronounced impact on the intestinal ecosystem by driving an expansion of facultative anaerobic bacteria at the cost of obligate anaerobic microbiota. This pathogen "blooming" is also a hallmark of enteric *Salmonella enterica* serovar Typhimurium (*S.* Tm) infection. Here, we analyzed the contribution of bacterial and host factors to *S.* Tm "blooming" in a gnotobiotic mouse model for *S.* Tm-induced enterocolitis. Mice colonized with the Oligo-Mouse-Microbiota (OMM^{12}), a minimal bacterial community, develop fulminant colitis by day 4 after oral infection with wild-type *S.* Tm but not with an avirulent mutant. Inflammation leads to a pronounced reduction in overall intestinal bacterial loads, distinct microbial community shifts, and pathogen blooming (relative abundance >50%). *S.* Tm mutants attenuated in inducing gut inflammation generally elicit less pronounced microbiota shifts and reduction in total bacterial loads. In contrast, *S.* Tm mutants in nitrate respiration, salmochelin production, and ethanolamine utilization induced strong inflammation and *S.* Tm "blooming." Therefore, individual *Salmonella*-specific inflammation-fitness factors seem to be of minor importance for competition against this minimal microbiota in the inflamed gut. Finally, we show that antibody-mediated neutrophil depletion normalized gut microbiota loads but not intestinal inflammation or microbiota shifts. This suggests that neutrophils equally reduce pathogen and commensal bacterial loads in the inflamed gut.

KEYWORDS *Salmonella* colitis, microbiota, mouse model, nutritional immunity

Salmonella enterica serovar Typhimurium (*S.* Tm) is a frequent cause of Salmonellosis in humans with millions of infections worldwide (1). The infection is usually self-limiting; however, in very young, old, or immunocompromised patients, *S.* Tm can induce life-threatening systemic disease with several thousands of deaths per year (2). The intestinal microbiota efficiently lowers the risk of infection by mediating colonization resistance (CR). When CR is reduced such as upon antibiotic therapy (3), a high-fat meal (4), or an infant or low-complex microbiota (5), *S.* Tm can invade the gut ecosystem and cause disease. In mice, the infection proceeds in several phases (6): First, *S.* Tm expands to high numbers in the gut by consuming hydrogen (7), diet- and microbiota-liberated mucosal carbohydrates (8, 9), oxygen (10), anaerobic electron acceptors, and fumarate (11, 12). Only after reaching a certain density (>10^5 CFU/g), *S.* Tm invades the gut mucosa at sufficient numbers and triggers intestinal inflammation (13, 14).

Gut inflammation dramatically alters the intestinal environment, leading to drastic changes in microbial community composition and favoring the *S.* Tm overgrowth (*Salmonella* "blooming") over obligate anaerobic commensal bacteria (15, 16). Evidently, *Salmonella* "blooming" is caused by two contrasting effects of inflammation (17, 18): (i)

Editor Manuela Raffatellu, University of California San Diego School of Medicine, La Jolla, California, USA

Address correspondence to Bärbel Stecher, stecher@mvp.lmu.de.

The authors declare no conflict of interest.

See the funding table on p. 15.

Received 17 August 2023
Accepted 5 December 2023
Published 8 January 2024

Copyright © 2024 American Society for Microbiology. All Rights Reserved.

selective fostering of pathogen growth by nutritional changes and (ii) differential killing of the mostly anaerobic commensal microbiota by innate immune defense mechanisms against which *Salmonella* is more resistant. In this study, we analyzed the contribution of both bacterial and host factors to *Salmonella* "blooming" in a gnotobiotic mouse model for *S*. Tm-induced enterocolitis.

An increase in the concentration of luminal oxygen levels, as well as anaerobic electron acceptors generated by the inflamed mucosa (10, 19), favors *S*. Tm growth over exclusively fermenting anaerobes (11, 20). This enables the pathogen to consume host-, diet-, and microbiota-derived metabolites, including mucin-derived sugars, ethanolamine, 1,2-propanediol, fructose-asparagine, succinate, and lactate (21–26), and gain a competitive advantage over competing commensals. The production of the siderophore salmochelin, a glycosylated variant of enterochelin that is not bound by the antimicrobial protein lipocalin 2 (LCN-2), also boosts *S*. Tm in the inflamed gut (27). On the other hand, acute *S*. Tm inflammation also exerts significant "collateral damage" to the beneficial microbiota (28). The microbiota is inhibited by antimicrobial molecules (27, 29) and bile salts (30), against which *Salmonella* exhibits a higher degree of resistance.

Moreover, neutrophils that are a hallmark of acute *Salmonella*-induced inflammation (31, 32) infiltrate the mucosa where they effectively reduce pathogen tissue loads by an NADPH-oxidase-mediated defense (13, 33). Transmigrated live neutrophils, which engulf luminal *S*. Tm, are present in the gut lumen early after infection (34). Neutrophils also form intraluminal structures ("casts" or pseudomembranes), which encapsulate commensals and thus prevent their epithelial contact and translocation (35). In *S*. Tm infection, luminal neutrophils impose a drastic bottleneck upon the pathogen population (36) and are likely to also kill commensals. In particular, the neutrophil effector molecules LCN-2, calprotectin, and elastase have been associated with microbiota alterations in response to pathogen-induced inflammation in mice (37, 38).

Overall, selective nutritional use and differential killing sustain long-term *S*. Tm "blooming" and the establishment of a "supershedder" state, that is, individuals that show high pathogen loads in stool (39). However, the relative importance of these contributing effects to *S*. Tm "blooming" remains elusive as previous studies focused on individual mechanisms and used different experimental protocols and *S*. Tm strains. Moreover, it is challenging to disentangle inflammation- and antibiotic-induced changes in the microbiome in models that rely on antibiotic pretreatment. To overcome this limitation, we analyzed the course of *S*. Tm-induced inflammation in a gnotobiotic infection model that does not rely on antibiotic pretreatment. Mice stably colonized with the Oligo-Mouse-Microbiota (OMM^{12}; 12 mouse-derived commensals) exhibit partial colonization resistance and develop *S*. Tm gut inflammation after oral infection (40). Members of the OMM^{12} are well studied with regard to their ecology and metabolic potential and can also be studied in *in vitro* community culture models (41, 42). Moreover, metabolic and immune phenotypes of OMM^{12} mice have been extensively characterized in comparison to germ-free and specific pathogen free (SPF) mice (43, 44). Therefore, this model is widely used and steadily gaining ground in research of colonization resistance against pathogens (4, 9, 45) or the functional study of other members of the gut microbial community, including bacteria, phages, and fungi (46–49). Here, we provide a detailed characterization of enteric *S*. Tm infection and its effect on the gut microbial community in the OMM^{12} model. We study the course of infection of different *S*. Tm mutants and assess their ability to cause inflammation-induced *S*. Tm "blooming." Finally, we employ a neutrophil depletion protocol to address the role of neutrophils in *S*. Tm "blooming," luminal bacterial killing, and microbiota alterations.

RESULTS

Course of oral *S*. Tm infection in OMM^{12} mice

Mice stably colonized with the OMM^{12} community (OMM^{12} mice) were infected intragastrically with 5×10^7 CFUs of either wild-type *S*. Tm (*S*. Tm^{WT}) or an avirulent *S*. Tm mutant (*S*. Tm^{avir}; Δ*invG*; *sseD::aphT*) lacking functional *Salmonella* pathogenicity island

(SPI)-1- and SPI-2-encoded type III secretion systems (T3SS). At days 1–4 post infection (p.i.), groups of mice were sacrificed, and intestinal and organ samples were taken for analyses (Fig. 1A). Cecum loads of both *S*. Tm strains increased steadily from day 1 to day 4 p.i. No difference was observed between *S*. Tm^{avir} and *S*. Tm^{WT} loads at all tested days ($P > 0.05$, Kruskal–Wallis test with Dunn's multiple comparison test; Fig. 1B). Compared to *S*. Tm^{avir}, *S*. Tm^{WT} loads were higher at day 4 p.i. in the mesenteric lymph nodes (mLNs; $P < 0.01$, Fig. 1C). No significant difference could be detected in the spleen ($P > 0.05$; Fig. 1E). Starting at day 3 p.i., *S*. Tm^{WT} caused strong gut inflammation as determined by vastly increased cecal LCN-2 levels (Fig. 1F) and cecal histopathology (Fig. 1G). Mice infected with avirulent *S*. Tm did not exhibit overt pathological changes in the cecum or increased LCN-2 (Fig. 1F and G).

S. Tm ^{WT} infection leads to pathogen blooming, a decrease in gut luminal bacterial load, and community shifts

Next, we determined the OMM^{12} community composition including *S*. Tm loads in cecum content (Fig. 2; Fig. S1) and feces (Fig. S2) by strain-specific quantitative PCR (qPCR). Calculations of relative abundance revealed that *S*. Tm^{WT} dominated (rel. abundance >50%) the bacterial community in feces and cecum content by day 4 p.i. (Fig. 2A through C; Fig. S2A through C), coinciding with developing gut inflammation (Fig. 1F and G). In contrast, no significant increase in relative abundance over time was observed for *S*. Tm^{avir} (Fig. 2A through C; Fig. S2A through C). ADONIS permutational multivariate analysis of variance (PERMANOVA) analysis on the Bray–Curtis distance metric revealed significant differences of microbial community composition by day and between *S*. Tm^{WT}- and S. Tm^{avir}-infected mice in feces and cecal content (Fig. 2AB; Fig. S2A and B; Tables S1 and S2). Strikingly, *S*. Tm^{WT} infection and resulting inflammation led to a drastic decrease in total gut bacterial loads determined by 16S rRNA copies (Fig. 2D; Fig. S2D). This was the case for the majority of OMM^{12} strains but *Enterococcus faecalis* KB1 (Fig. S1).

We also infected OMM^{12} mice with *S*. Tm mutants in either the SPI-1 (*S*. Tm$^{\Delta SPI-1}$)- or the SPI-2 (*S*.Tm$^{\Delta SPI-2}$)-encoded T3SS for 4 days. We compared *S*. Tm loads and microbiota composition to *S*. Tm^{WT} and *S*. Tm^{avir} data shown in Fig. 1. *S*. Tm$^{\Delta SPI-1}$ and *S*. Tm$^{\Delta SPI-2}$ colonized the intestine at largely similar levels (Fig. S3A). Interestingly, systemic *S*. Tm loads were similar between the mutants (Fig. S4A through C). *S*. Tm$^{\Delta SPI-2}$ (triggering gut inflammation via the SPI-1 T3SS) induced more cecal pathology and higher *S*. Tm abundance compared to the SPI-1-deficient mutant although this difference was not statistically significant (Fig. S3B and C). Microbiota composition in the cecum content was significantly different between all groups, as determined by ADONIS PERMANOVA analysis on the Bray–Curtis distance metric (Fig. S3E; Table S3). Blooms were only evident in *S*.Tm$^{\Delta SPI-2}$- and *S*. Tm^{WT}-infected mice (Fig. S3F). The total bacterial load in *S*.T m$^{\Delta SPI-1}$- and *S*. Tm$^{\Delta SPI-2}$-infected mice was altered when compared to *S*. Tm^{avir} but not significantly changed when compared to the S. Tm^{WT}-infected group (Fig. S3G). This applied also for most of the individual OMM^{12} strains (Fig S4D through O). Taken together, *S*. Tm^{WT} induced strong gut inflammation in OMM^{12} mice, beginning at day 3 p.i. and depending on the activity of both *Salmonella* T3SS. Severe inflammation at day 4 p.i. was paralleled with *S*. Tm^{WT} blooming, drastic reduction of total gut luminal bacterial loads, and overall changes in microbiota composition.

Anaerobic respiration and ethanolamine utilization fuel *S*. Tm blooms and dysbiosis

To analyze the relevance of anaerobic and aerobic respiration for *S*. Tm blooming, we generated *S*. Tm mutants deficient in nitrate respiration (*S*. Tm$^{Ni.}$; Δ*narZ*; *narG::cat*; *napA::aphT*) and in nitrate and tetrathionate respiration (*S*. Tm$^{Ni.\ +\ Te.}$; Δ*narZ*; *narG::cat*; *napA::aphT*; *ttrS::tet*). Moreover, to probe the role of siderophore-mediated iron acquisition and ethanolamine utilization, we generated *S*. Tm *entA*::cat (*S*. Tm^{EntA}) and *eutC::aphT* mutant (*S*. Tm^{EA}) strains. In addition, we created an *S*. Tm *cyxA* mutant, attenuated in aerobic respiration by the deletion of the cytochrome bd-II oxidase gene (*S*. Tm^{cyx}; Δ*cyxA*).

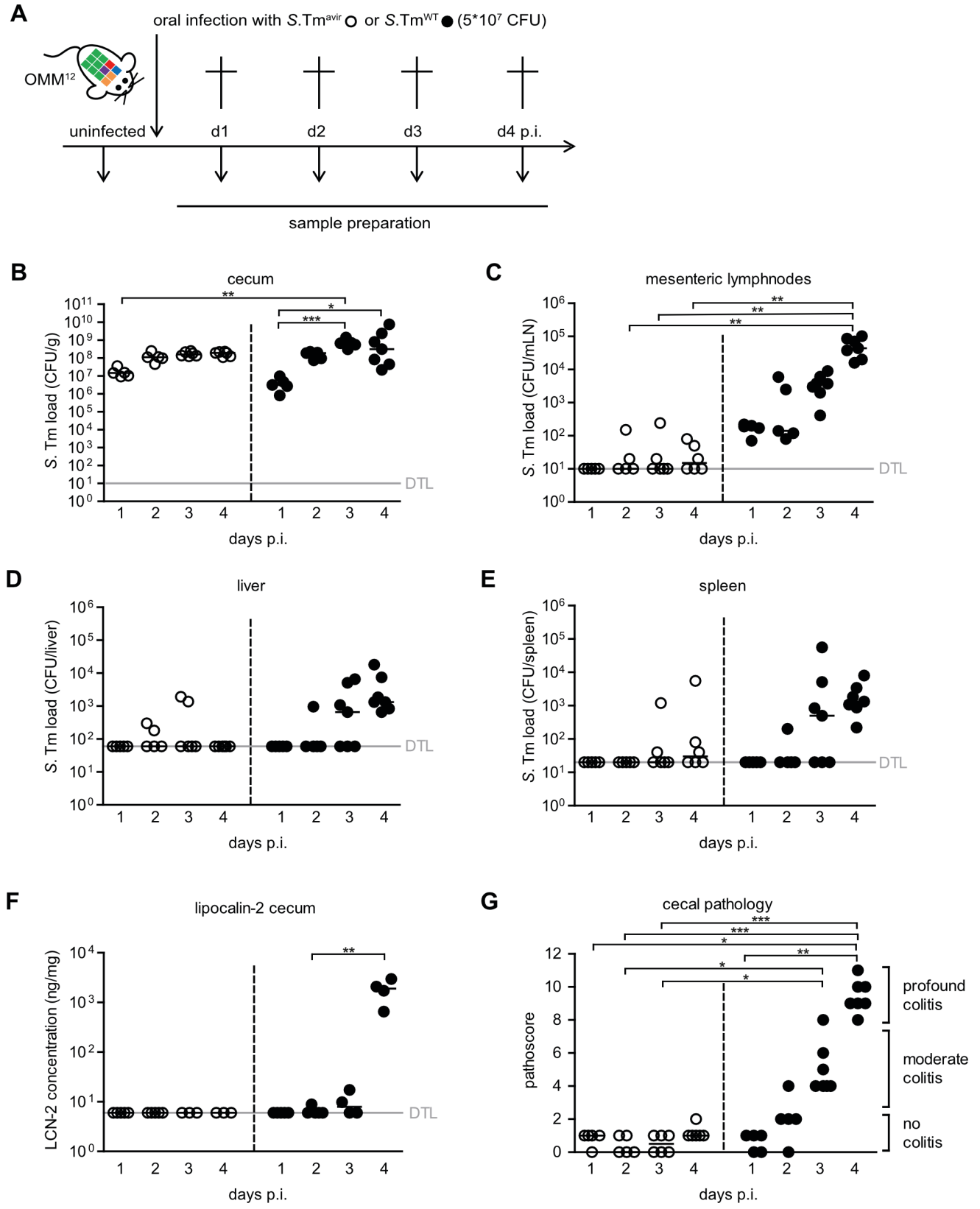

FIG 1 Course of enteric *S.* Tm infection and systemic dissemination. (A) Experimental scheme. OMM[12] mice were orally infected with either *S.* Tm[avir] or *S.* Tm[WT]. Mice were sacrificed at days 1, 2, 3, and 4 p.i. (infection with *S.* Tm[avir]: day 1 p.i. $n = 5$, day 2 p.i. $n = 5$, day 3 p.i. $n = 6$, and day 4 p.i. $n = 6$; infection with *S.* Tm[WT]: day 1 p.i. $n = 5$, day 2 p.i. $n = 5$, day 3 p.i. $n = 7$, and day 4 p.i. $n = 7$). *S.* Tm loads in (B) cecal content, (C) mLNs, (D) liver, and (E) spleen were determined by plating. (Continued on next page)

FIG 1 (Continued)

(F) LCN-2 amount in cecal content d4 was determined by enzyme-linked immunosorbent assay (ELISA). (G) Histopathological analysis of cecal tissue. Cecal tissue sections of the mice were stained with hematoxylin/eosin to determine the degree of submucosal edema, neutrophil infiltration, and epithelial damage (1–3: no pathological changes; 4–6: moderate inflammation; and above 7: severe inflammation). Statistical analysis was performed using Kruskal–Wallis test with Dunn's multiple comparison test (*P < 0.05, **P < 0.01, and ***P < 0.001). Each dot represents one mouse, black lines indicate median, and gray lines indicate detection limit (DTL).

We infected groups of OMM^{12} mice with 5×10^7 CFUs of the mutant strains or *S.* Tm^{WT}. Fecal samples were collected on different days after infection in order to monitor the course of intestinal *S.* Tm colonization. Mice were sacrificed at day 4 p.i., cecal content was harvested for microbiota analysis, inflammation was quantified, and systemic *Salmonella* loads were determined (Fig. 3). *S.* Tm strains colonized the gut of OMM^{12} mice equally well (Fig. 3A). Only *S.* Tm^{EA} showed significantly reduced loads at day 3 p.i. compared to *S.* Tm^{WT} (P < 0.01, Kruskal–Wallis test with Dunn's multiple comparison test; Fig. 3A). There was no difference in systemic *Salmonella* loads at day 4 p.i. between groups (Fig. S5). *S.* Tm^{WT}, *S.* Tm^{EA}, and *S.* Tm^{EntA} induced profound colitis by day 4 p.i., while *S.* Tm$^{Ni.+Te}$ induced significantly less colitis symptoms (P < 0.001, Fig. 3B). For *S.* Tm^{cyx}, no significant differences could be detected in pathogen loads in intestine or organs in comparison to *S.* Tm^{WT} (Fig. S6). PERMANOVA analysis with ADONIS on the Bray–Curtis distance metric revealed significant differences between the cecal community structures of *S.* Tm$^{Ni.+Te}$ and *S.* Tm^{WT} or *S.* Tm^{EntA}-infected mice (Fig. 3D; Table S4) and abundance of most OMM^{12} bacteria was increased in *S.* Tm$^{Ni.+Te}$-infected mice (Fig. S7). For *S.* Tm^{cyx}, no significant difference was found with respect to microbiota composition in comparison to *S.* Tm^{WT} (Fig. S6 and S7; Table S5). *S.* Tm$^{Ni.+Te}$ mutant did not establish "blooms," while relative abundances of the other *S.* Tm mutants were similar to *S.* Tm^{WT} (Fig. 3E), and total bacterial loads were increased in mice infected with *S.* Tm$^{Ni.+Te}$ compared to *S.* Tm^{WT}-infected mice (Fig. 3F).

Neutrophils reduce overall luminal bacterial loads but do not promote *Salmonella* "blooms"

Next, we set out to test the hypothesis that neutrophils are the cause of decreased luminal bacterial loads in *S.* Tm^{WT}-infected OMM^{12} mice at day 4 p.i. Therefore, we employed a neutrophil depletion protocol using α-Ly6G and α-G-CSF antibodies or isotype control antibodies in OMM^{12} mice that were additionally infected with *S.* Tm^{WT} (Fig. 4A). Antibody-mediated depletion was confirmed by fluorescence activated cell sorting (FACS) analysis of blood samples gating on CD45$^+$, SYTOX$^-$, CD3$^-$, CD11b$^+$, Ly-6G$^+$, and Ly-6C^{intermediate} cells and by quantifying neutrophil-elastase in cecal content (Fig. 4B). Only mice with confirmed neutrophil depletion (<4% Ly6G$^+$/CD45$^+$ cells) were included in the analysis.

Some neutrophil-depleted mice developed severe infection and had to be euthanized at day 2 or 3 p.i. (indicated with gray and black arrows). Cecal *S.* Tm^{WT} loads were similar in both groups of mice at days 1–3 p.i. but significantly higher in neutrophil-depleted mice at day 4 p.i. (Fig. 4C). At the point of sacrifice, all mice developed pronounced gut inflammation as determined by LCN-2 levels (Fig. 4D). Systemic loads of *S.* Tm^{WT} were higher in the mLN, spleen, and liver of neutrophil-depleted mice (Fig. S8A through C).

There was no apparent difference in the overall cecal microbiota composition between the groups at day 4 p.i. (Fig. 4E and F; Table S6). Moreover, no difference in rel. *S.* Tm^{WT} abundance was observed between the groups (Fig. 4G). However, a lower overall amount of total gut luminal bacteria was observed in the isotype group (Fig. 4H copies/mg content isotype vs depleted P < 0.001, Mann–Whitney U test), indicating that neutrophils are causal for inflammation-associated reduction of gut luminal bacterial loads in *S.* Tm-infected OMM^{12} mice. Reduction was most pronounced for *Bacteroides caecimuris* I48, *Muribaculum intestinale* YL27, *Akkermansia muciniphila* YL44, *Turicimonas*

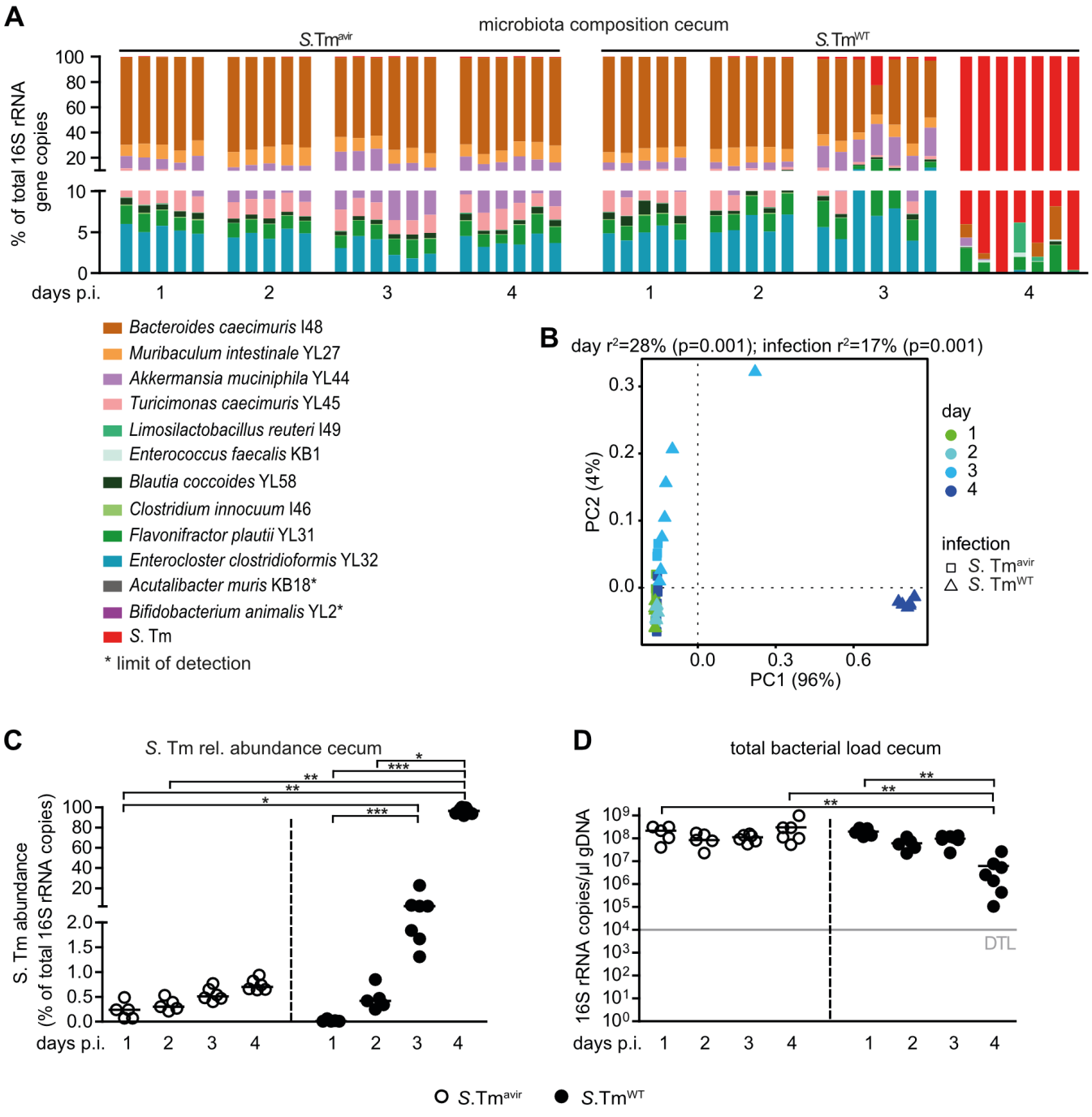

FIG 2 *S.* Tm^{WT} causes pronounced shifts in microbiota composition at day 4 p.i. in OMM^{12} mice. (A) Analysis of microbiota composition in cecal content. Microbiota composition was determined by strain-specific qPCR assay and is shown as relative abundances of the individual strains (% of cumulated 16S rRNA gene copy numbers). (B) Principal coordinates analysis (PCoA) based on the distance matrix of Bray–Curtis dissimilarity of relative OMM^{12} abundance profiles shows the effect of time after infection. Points are colored by time (days) after infection. (C) Relative abundance of *S.* Tm in cecal contents at different time points. (D) Absolute amount of 16S rRNA gene copies (determined by a universal primer/probe combination). Statistical analysis was performed using Kruskal–Wallis test with Dunn's multiple comparison test (*P<0.05, **P < 0.01, and ***P < 0.001). Each dot represents one mouse, black lines indicate median, and gray lines indicate DTL.

muris YL45, *Blautia coccoides* YL58, *Flavonifractor plautii* YL31, and *Enterocloster clostridioformis* YL32—other bacteria were less affected (Fig. S8D through O).

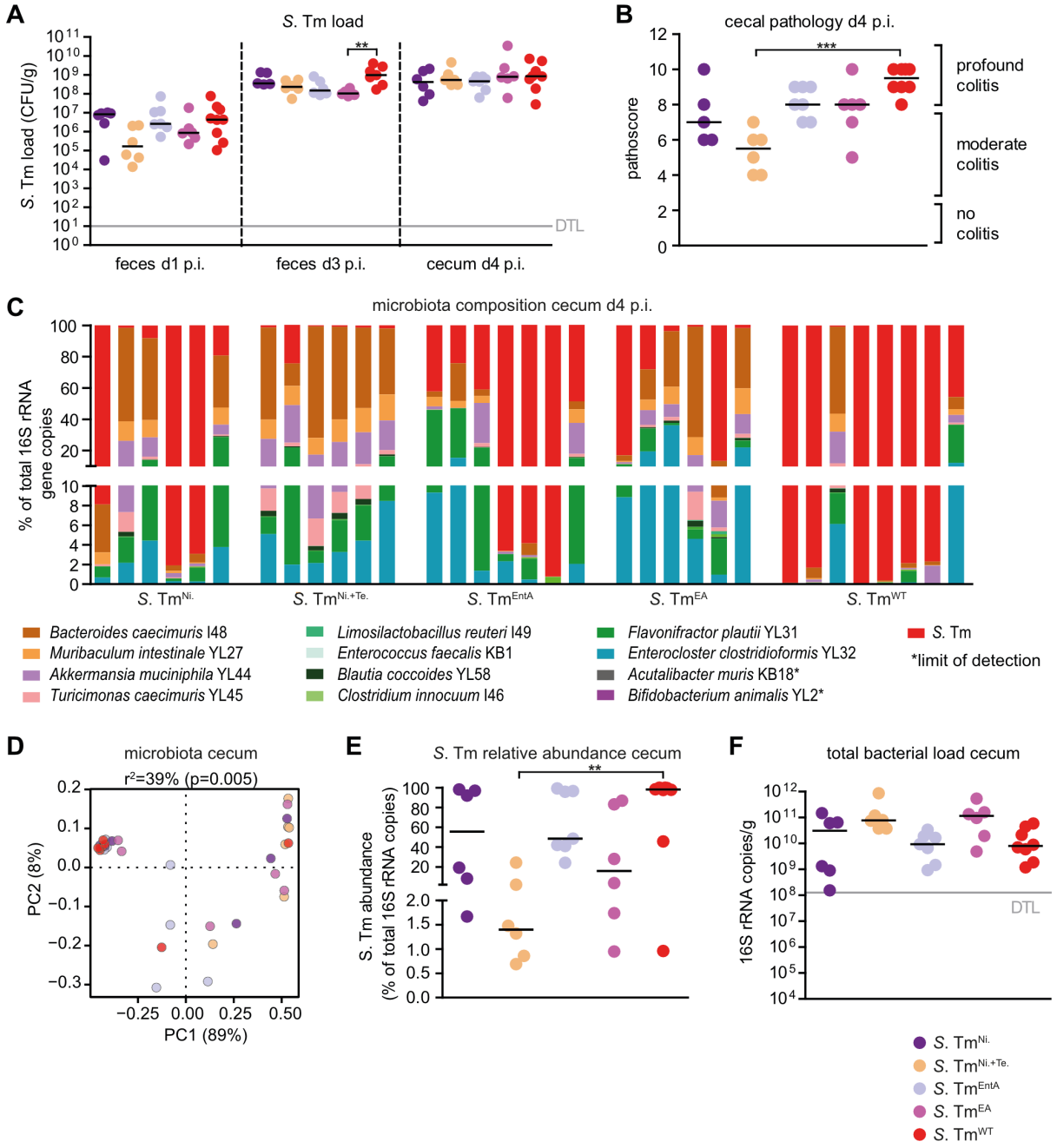

FIG 3 Course of infection of *S.* Tm mutants in anaerobic respiration, salmochelin production, and ethanolamine utilization in OMM^{12} mice. OMM^{12} mice were orally infected with different *S.* Tm mutant strains: *S.* Tm$^{Ni.}$ (n = 6), *S.* Tm$^{Ni.+Te.}$ (n = 6), *S.* Tm^{EntA} (n = 7), *S.* Tm^{EA} (n = 6), or *S.* Tm^{WT} (n = 8). Mice were sacrificed at day 4 p.i. (A) *S.* Tm loads in feces and cecal content at days 1, 3, and 4 p.i. were determined by plating. (B) Histopathological analysis of cecal tissue at day 4 p.i. Cecal tissue sections of the mice were stained with hematoxylin/eosin to determine the degree of submucosal edema, neutrophil infiltration, and epithelial damage (1–3: no pathological changes; 4–6: moderate inflammation; and above 7: severe inflammation). (C) Analysis of microbiota composition in cecal content. Microbiota composition was determined by strain-specific qPCR assay and is shown as relative abundances of the individual strains (% of cumulated 16S rRNA gene copy numbers). (D) PCoA based on the distance matrix of Bray–Curtis dissimilarity of relative OMM^{12} abundance profiles shows the effect of the different *S.* Tm mutant strains. Points are colored by time (days) after infection. (E) Relative abundance of *S.* Tm and (F) absolute amount of 16S rRNA gene copies (determined by a universal primer/probe combination) in cecal contents 4 days p.i. Statistical analysis was performed using Kruskal–Wallis test with Dunn's multiple comparison test (*P < 0.05, **P < 0.01, and ***P < 0.001). Each dot represents one mouse, black lines indicate median, and gray lines indicate DTL.

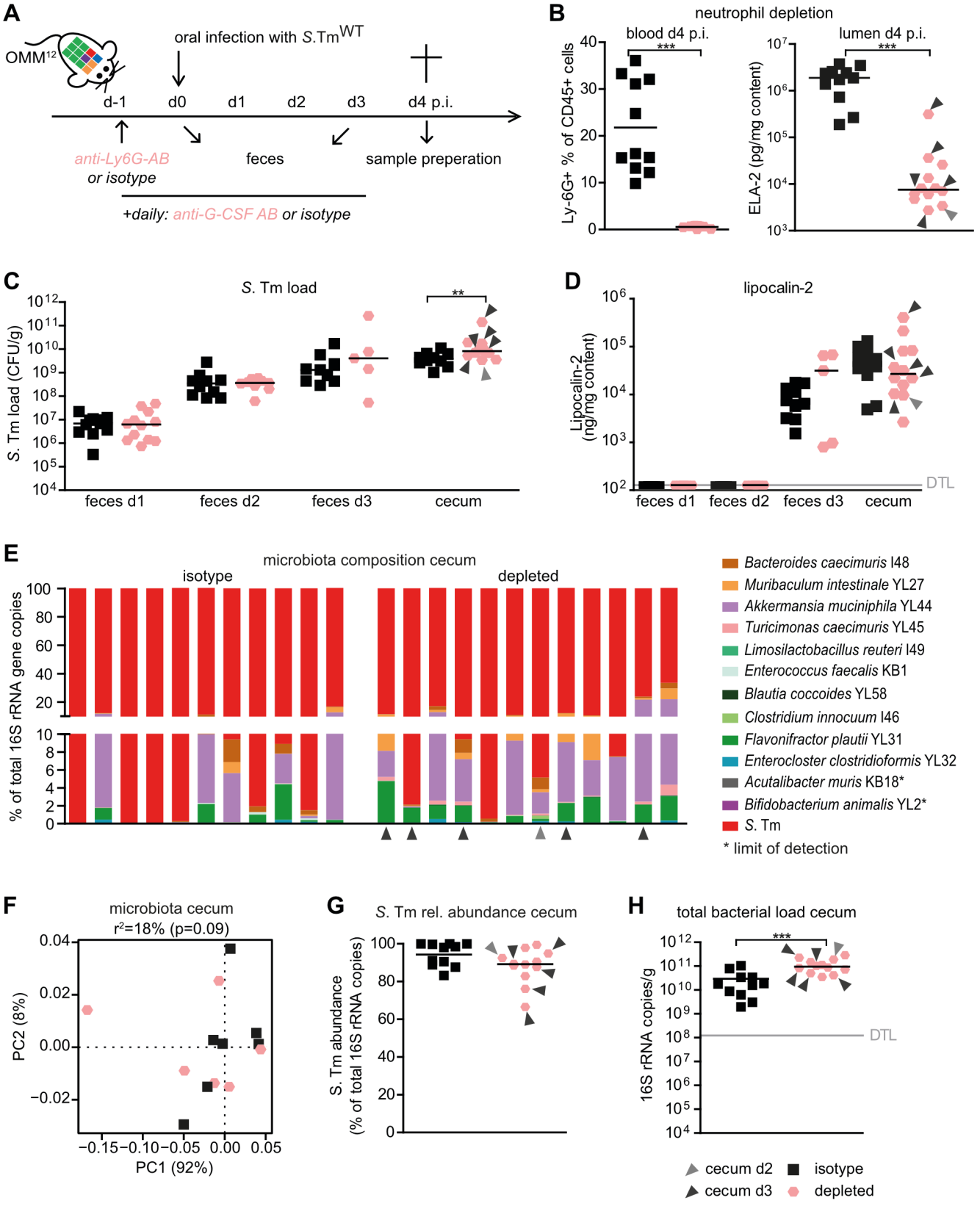

FIG 4 Neutrophils reduce the total gut luminal bacterial loads but are dispensable for the induction of *Salmonella* "blooms" and dysbiosis. (A) Experimental scheme. OMM[12] were treated with one dose of α-Ly6G antibody or isotype control 1 day before infection with *S.* Tm[WT]. In addition, α-G-CSF antibody or isotype control was daily administered starting from day −1 until day 3 p.i. All antibodies were given via the intraperitoneal route. (B) Monitoring of neutrophil depletion

(Continued on next page)

FIG 4 (Continued)

at day 4 p.i. in blood by FACS gating on $CD45^+$, $SYTOX^-$, $CD3^-$, $CD11b^+$, Ly-$6G^+$, and Ly-$6C^{intermediate}$ cells or in cecal content by neutrophil elastase-specific ELISA. FACS data are indicated as the mean. Statistical analysis was performed using the Mann–Whitney U test. (C) *S.* Tm loads in feces at days 1, 2, and 3 and cecal content at day 4 p.i. were determined by plating. (D) LCN-2 levels in feces and cecal content (ng/mg content). LCN-2, elastase levels, and CFUs are shown as median, and data were analyzed using the Mann–Whitney U test. (E) Analysis of cecal microbiota composition at day 4 p.i. with different *S.* Tm^{WT} and neutrophil depletion or isotype control treatments. Microbiota composition is shown as relative abundance and expressed as % of cumulated 16S rRNA gene copy numbers. (F) PCoA based on the distance matrix of Bray–Curtis dissimilarity of relative OMM^{12} abundance profiles shows the effect of the different treatments. (G) Relative abundance of *S.* Tm and (H) absolute amount of 16S rRNA gene copies (determined by a universal primer/probe combination) in cecal contents 4 days p.i. Light and dark gray arrows indicate samples analyzed at day 2 or 3 p.i., respectively. Statistical analysis was performed using the Mann–Whitney U test (*$P < 0.05$, **$P < 0.01$, and ***$P < 0.001$). Each dot represents one mouse, black lines indicate median, and gray lines indicate DTL.

DISCUSSION

Together, the host and its intestinal symbionts establish microbiota-nourishing immunity that forms an efficient barrier against *S.* Tm infection (50). Epithelial hypoxia, short-chain fatty acid production, and depletion of growth substrates are cornerstones of this barrier. Using its virulence factors, *S.* Tm can overcome colonization resistance, trigger inflammation, and alter the gut luminal environment to benefit from it—at the expense of intestinal commensal bacteria. Inflammation-driven pathogen "blooming" has a major impact on *S.* Tm dissemination and evolution (51). Overgrowth of related Enterobacteriaceae promotes the exchange of conjugative plasmids (52) and phages (53). This increases the chance of spreading antibiotic resistances and fosters evolution of highly virulent strains (54), emphasizing the broad implications of *S.* Tm adaptation of the inflammatory milieu in the mammalian gut. Here, we analyze the extent to which *S.* Tm-induced intestinal inflammation, virulence, and gut luminal neutrophils contribute to alterations in the gut microbiota loads and community profiles in OMM^{12} mice, a widely used infection model (4, 9, 55) based on a well-characterized minimal bacterial community (56).

Due to the partial colonization resistance phenotype of OMM^{12} mice, wild-type *S.* Tm induced severe gut inflammation within 4 days after oral infection without antibiotic pretreatment. Mice were characterized by an overall reduction of luminal bacterial loads and *S.* Tm blooming (i.e., *S.* Tm being the dominant species). This overgrowth was not observed with an avirulent mutant (Δ*invG* Δ*ssaV*; *S.* Tm^{avir}), which can colonize the gut but is defective in inducing inflammation. This confirms the results from previous studies in the streptomycin-treated mouse colitis model and highlights the pronounced negative impact of intestinal inflammation on the majority of intestinal commensals while fostering pathogen overgrowth (15).

Comparing the course of infection in *S.* Tm TTSS mutants, we found that *S.* $Tm^{\Delta SPI\text{-}1}$ was more strongly attenuated in inducing gut inflammation than *S.* $Tm^{\Delta SPI\text{-}2}$ at day 4 p.i. This suggests that in OMM^{12} mice, the SPI-1 TTSS contributes more to overall inflammation than the SPI-2 TTSS. Previous work in the streptomycin model showed that SPI-1 triggers inflammation within hours after infection. This response is due to effector proteins that initiate a complex immunological signaling cascade, culminating in the production of IFNγ (57–61). In contrast, in OMM^{12} mice, overt inflammation starts only by day 3 p.i. (Fig. 1F and G), which is mainly due to initially lower *S.* Tm loads ($<10^7$ CFU/g) compared to streptomycin-treated mice ($>10^8$ CFU/g). Mutants lacking a functional SPI-1 or a SPI-2 TTSS caused equally attenuated colitis at day 4 p.i. However, at early time points postinfection (days 1 and 2 p.i.), the *S.* $Tm^{\Delta SPI\text{-}1}$ mutant is strongly attenuated and inflammation triggered via the SPI-2 TTSS only developed at day 3 p.i. (62).

S. Tm mutants in anaerobic respiration as well as iron uptake via salmochelin and ethanolamine utilization were previously shown to be attenuated in growth in the inflamed gut in direct competition with *S.* Tm^{WT} (11, 20, 27, 63). In this study, we aimed to identify mechanisms that promote *S.* Tm blooming in competition against the OMM^{12} microbiota. We show that a double mutant in anaerobic nitrate and tetrathionate respiration (*S.* Tm^{Ni+Te}) has a reduced capacity to bloom and induce microbial community

shifts. As gut inflammation in *S.* Tm^{Ni+Te}-infected mice was also significantly reduced at day 4 p.i., we cannot conclude that anaerobic respiration creates an advantage in competition against OMM^{12} in the inflamed gut. In contrast, mutants in O_2 and nitrate respiration, ethanolamine utilization, and salmochelin production (*S.* Tm^{cyx}, *S.* Tm^{Ni}, *S.* Tm^{EA}, and *S.* Tm^{EntA}) induced strong inflammation, bloomed, and altered the microbiota composition to a similar extent as *S.* Tm^{WT}. Therefore, these mechanisms are, at least individually, not required for competition against OMM^{12} bacteria in the inflamed gut. In the previous work using the streptomycin-treated colitis model, *S.* Tm^{cyx} was strongly attenuated in intestinal colonization (10). While the phenotype of partial colonization resistance of OMM^{12} mice was key for conducting the experiments without previous microbiota perturbation, it also has its limitations. The OMM^{12} microbial community lacks key functional members, such as *Escherichia coli* or other facultative anaerobic bacteria that compete with *S.* Tm for nutrients and O_2 in the inflamed gut upon recovery from streptomycin treatment. To this end, a more complex microbial model community such as the recently established human-derived defined complex communities might be used (64).

Our data indicate that neutrophils protect the host from systemic Salmonella spread and reduce total gut luminal bacterial loads but do not contribute to *Salmonella* "blooms" and concomitant dysbiosis. Notably, antibody-mediated depletion of neutrophils resulted in the reduction of LCN-2 and elastase-2 levels and concomitantly resulted in an overall increase in total gut luminal bacterial loads. This confirms the pronounced antibacterial function of transmigrated neutrophils in the gut lumen reported previously (34, 35, 37). In contrast, neutrophil depletion did not change the relative abundance of gut luminal *S.* Tm. This suggests that neutrophil-derived antimicrobial effectors equally reduce numbers of *S.* Tm and members of the OMM^{12} and are not causally involved in *S.* Tm blooming in this model. Rather, "blooming" is mainly mediated by the pathogens' diverse capabilities of taking advantage of the altered substrate range in the inflamed intestine.

Gnotobiotic OMM^{12} mice are increasingly used as a standardized infection model for *S.* Tm and other pathogenic Enterobacteriaceae (4, 9, 45). Here, we present a detailed characterization of the course of *S.* Tm^{WT} infection and mutants in major virulence factors. Our study reveals that OMM^{12} mice infected with *S.* Tm^{WT} develop fulminant colitis by day 4 p.i. characterized by pathogen blooming and shifts in microbiota composition. We conclude that OMM^{12} mice are a valuable model to dissect the impact of *S.* Tm^{WT}-induced inflammation on the gut ecosystem, including all its members, without the need for previous microbiota perturbation.

MATERIALS AND METHODS

Bacterial strains

For detailed information about individual Oligo-MM^{12} strains refer to reference (40). All Oligo-MM^{12} strains are part of the mouse intestinal bacteria collection [miBC (65)] and are also available via the German Collection of Microorganisms and Cell Cultures (www.dsmz.de/miBC). *Salmonella* strains used and created in this study are based on *S.* Tm strain SL1344 (Table 1).

Construction of *S.* Tm strains and plasmids

All bacterial strains used in this study are listed in Table 1. *S.* $Tm^{Ni.}$ (MBE7: Δ*narZ*, *narG::cat*, *napA::aphT*) was generated in a stepwise manner. First, single *S.* Tm mutant strains were generated (MBE1: *narZ::cat*, MBE2: *narG::cat* and MBE3: *napA::aphT*) using λ red recombination as described previously (69). Briefly, antibiotic resistance genes as well as flippase recognition target (FRT) sites were PCR-amplified using specific knock out primers (ko-primers, Table 2) and the plasmids pKD3 (*cat*) or pKD4 (*aphT*) listed in Table 3. PCR products were subsequently electroporated into *S.* Tm^{WT} harboring pKD46 (Table 3). The

TABLE 1 Bacterial strains used in this study

Strain	Strain ID	Genotype	Reference
S. Tm^{WT}	SB300	*S.* Tm strain SL1344	(66)
S. Tm^{Avir}	M557	Δ*invG; sseD::aphT*	(67)
S. Tm^{SPI-1}	SB161	Δ*invG*	(68)
S .Tm^{SPI-2}	M556	*sseD::aphT*	(67)
MBE1	MBE1	*narZ::cat*	This study
MBE2	MBE2	*narG::cat*	This study
MBE3	MBE3	*napA::aphT*	This study
MBE4	MBE4	*narZ::cat*	This study
MBE5	MBE5	Δ*narZ*	This study
MBE6	MBE6	Δ*narZ*; *narG::cat*	This study
S. Tm$^{Ni.}$	MBE7	Δ*narZ*; *narG::cat*; *napA::aphT*	This study
S. Tm$^{Ni. + Te.}$	MBE8	Δ*narZ*; *narG::cat*; *napA::aphT*; *ttrS::tet*	This study
MBE9	MBE9	*entA::cat*	This study
S. Tm^{EntA}	MBE10	*entA::cat*	This study
MBE11	MBE11	*eutC::aphT*	This study
S. Tm^{EA}	MBE12	*eutC::aphT*	This study

narZ::cat allele from MBE1 was transduced to *S.* Tm^{WT} by P22-transduction (70) in order to create MBE4. The *narZ::cat* was then deleted using flippase (FLP)-recombinase encoded on pCP20 (Table 3). The resulting strain MBE5 (Δ*narZ*) was transduced with P22-phage lysate of MBE2 in order to create MBE6 (Δ*narZ*, *narG::cat*). MBE6 was finally transduced with P22-phage lysate of MBE3 to generate MBE7 (Δ*narZ*, *narG::cat*, *napA::aphT*). In order to construct *S.* TmNi.$^{Ni. + Te.}$ (MBE8: Δ*narZ*, *narG::cat*, *napA::aphT*, *ttrS::tet*), the *ttrS::tet* allele from *S.* Tm stain M961 [Δ*sodCI*, Δ*sodCII*, *BCB4::tet* (71)] was P22-transduced into MBE7. *S.* Tm^{EntA} (MBE10: *entA::cat*) was created by P22-transduction of the *entA::cat* allele from MBE9 to *S.* Tm^{WT}. MBE9 was previously generated by λ red recombination. *S.* Tm$^{EA.}$ (MBE12: *eutC::aphT*) was constructed by P22-transduction of the *eutC::aphT* allele from MBE11 to *S.* Tm^{WT}. MBE11 was generated before using λ red recombination. In all cases, genetic modifications were verified by PCR using gene-specific check-up primers (Table 2). The construction and sequences of plasmids harboring full-length 16S rRNA sequences used as standard for qPCR reactions are detailed in reference (40).

Culture conditions and bacterial *in vitro* assays

Culture conditions as well as cryopreservation protocols of individual Oligo-MM^{12} strains are described in reference (40). For mouse infection, a single colony of an *S.* Tm strain was inoculated in 3 mL of lysogeny broth (LB) medium containing 0.3 M NaCl (LB$^{0.3}$) and grown on a wheel rotor for 12 h at 37°C. The starter culture was diluted in a 1:20 ratio in fresh LB$^{0.3}$ and incubated for another 4 h at 37°C under constant rotation. The subculture was washed in ice-cold phosphate-buffered saline (PBS), and the pellet was subsequently re-suspended in PBS. Mice were finally gavaged with 5×10^7 CFUs of *S.* Tm strains. For investigating phenotypes conferred by gene knock outs, individual colonies of *S.* Tm strains were aerobically inoculated with 5 mL of M9 medium ($Na_2HPO_4 \cdot 2H_2O$ 40 mM, KH_2PO_4 20 mM, NaCl 9 mM, NH_4Cl 37.39 mM, D-glucose 1.1 mM, $MgSO_4$ 1 mM, $CaCl_2$ 100 µM, Thiamine 10 mg/mL, and Histidine 500 mg/L) without antibiotics on a wheel rotor for 12 h at 37°C. Aerobic as well as anaerobic (7% H_2, 10% CO_2, and rest N_2) subcultures with a starting OD_{600} of 0.02 were subsequently carried out in 10 mL of M9 medium with and without nitrate (20 mM). For testing *S.* Tm strains deficient in ethanolamine utilization, the M9 medium was additionally supplemented with ethanolamine (5 mM) and tetrathionate (40 mM). Aerobic subcultures were performed in glass Erlenmeyer flasks sealed with aluminum foil, whereas anaerobic subcultures were conducted in 100 mL Wheaton glass serum bottles with pre-reduced medium (pre-reduction for at least 2 days under anoxic conditions: 3% H_2 and rest

TABLE 2 Primers used for construction of *Salmonella* mutants[a]

Designation	Sequence 5′–3′	Construction of	Amplicon size (bp)
narZ-fwd-ko	AATGGTTTAACGCCAAATCGACAGGATGGCGGAAAATTTATCGAAGCAGGAGAAATGTCatatgaatatcctccttagtt		
narZ-rev-ko	GGTGTGACAGCCAATACATTTATCGAGATTCAGTACCATCCCAACCTGTGAGCGTATTTtgtgtaggctggagctgcttc	MBE1 (*narZ*::*cat*)	
narZ fwd-check up	GCGTCGTAAGCCTAAACA		
narZ rev-check up	CCGGTCCAGACGTTTTTA		3,948
narG-fwd-ko	CTTAGTTAAGCAATGTCGATTTATCAGAGAGCCGTAAGGTTCCACACAGGAGAAACCCGatatgaatatcctccttagtt		
narG-rev-ko	GGTATGACAGCCGATGCACTTATCGAGATTCAGCACCATGCCGACTTGTGAACGAATTTtgtgtaggctggagctgcttc	MBE2 (*narG*::*cat*)	
narG fwd-check up	TTCTCACGCCCATTCAGC		
narG rev-check up	CCAGACGTTTTTACAGGT		3,921
napA-fwd-ko	GGCGTACTGGCGGTGTCGCTGGTTTATCACCAGCAGGATGAGCAAGGTGAGGAAACACCatatgaatatcctccttagtt		
napA-rev-ko	ACATCACGCAGGAAGCGGCGGCGGCCATTTTGGGGTTTCGCTGTACGGGACATAACGCGtgtgtaggctggagctgcttc	MBE3 (*napA*::*aphT*)	
napA fwd-check up	ACAATTGAGTCAGTACGC		
napA rev-check up	GCTGGCGAAGACATTTTC		2,756
ttrS fwd-check up	CGGCTTGTTGTTGATCTAA		
ttrS rev-check up	CCCAGACTTTCCAGTAAAA		1,873
entA-fwd-ko	CTGGCGAAAAACCCGACCATTGACGCCTGGTGGGCGCTGCTTTCTCGCGGGGTAGAGTAatatgaatatcctccttagtt		
entA-rev-ko	AGTGTTCTGACTGGTAGCGTTCAATTCATCCAGCGTTAAATGCCGTTTCCAGATCATCGtgtgtaggctggagctgcttc	MBE9 (*entA*::*cat*)	
entA fwd-check up	GTAAAGTACACGGCGATAT		
entA rev-check up	TAAACAATGCCCAGATGCG		932
eutC-fwd-ko	GTCTGACCAAACGGGCGGGCGATCCGTCACTGTTCTTCTGATGACGCGGGGATAACACCatatgaatatcctccttagtt		
eutC-rev-ko	ATCACGCGCATGGCAGTCACTGAAGGTCGAATTAAATCTAATGCAGGCATGATGTCTCCtgtgtaggctggagctgcttc	MBE11 (*eutC*::*aphT*)	
eutC fwd-check up	CTGGAAACGATGGGCATTAT		
eutC rev-check up	TAATTTAAGTTCCCGCGCAA		1,086

[a]Genes of interest were replaced by either chloramphenicol (*cat*) or kanamycin (*aphT*) resistance genes using the λ red recombination system (69). PCR products were generated with primers harboring a homology region adjacent to the gene of interest (capital letters) and a sequence targeting the plasmids pKD3 (*cat*) and pKD4 (*aphT*, small letters). Check-up primers were used to verify the correct insertion of the antibiotic cassette.

TABLE 3 Plasmids used for λ red and FLP recombination

Plasmid	Function	Genotype	Reference
pKD3	Harbors a chloramphenicol resistance gene (*cat*)	*cat* with FRT sites, Amp^R	(69)
pKD4	Harbors a kanamycin resistance gene (*aphT*)	*aphT* with FRT sites, Amp^R	(69)
pKD46	Harbors 2,154 nt (31088–33241) of phage λ, enzymes for recombination	*araC*, ParaB γ, β and exo, $repA101^{ts}$, Amp^R	(69)
pCP20	Harbors FLP-recombinase	FLP^+, λ $cI857^+$, λ p_R Rep^{ts}, Amp^R, Cm^R	(72)

N_2). Subcultures were incubated at 37°C and shaken at 180 rpm, and samples were taken for OD_{600} measurement and determination of nitrate concentrations (73). *In vitro* competition assays were performed as described in reference (74). Briefly, starter cultures of the competing strains in 5 mL of LB or M9 medium without antibiotics incubated on a wheel rotor for 12 h at 37°C were mixed in a 1:1 ratio with a starting OD_{600} of 0.05 of each strain and used to inoculate 14 mL cultures with either plain mucin broth (Type II porcine mucin 2.5 g/L, Morpholino propanesulfonic acid sodium 9.25 g/L, $MgSO_4$ 2.2 mM, trace elements 1,000×: $CaCl_2 \cdot 2H_2O$ 0.3 mM, $ZnSO_4 \cdot 7H_2O$ 0.1 mM, $FeSO_4 \cdot 7H_2O$ 0.045 mM, Na_2SeO_3 0.2 mM, $Na_2MoO_4 \cdot 2H_2O$ 0.2 mM, $MnSO_4 \cdot H_2O$ 2 mM, $CuSO_4 \cdot 5H_2O$ 0.1 mM, $CoCl_2 \cdot 6H_2O$ 3 mM, and $NiSO_4 \cdot 6H_2O$ 0.1 mM) or mucin broth containing nitrate (40 mM). For competition assays underlining the importance of tetrathionate respiration, the mucin broth was supplemented with tetrathionate (40 mM) and histidine (500 mg/L) to enhance growth. Cultures were statically incubated in 15 mL plastic tubes for 24 h at 37°C. CFUs of *S.* Tm strains were determined by plating on LB agar plates containing selective antibiotics. The deficiency of acquiring iron via siderophores was investigated using Chromazurol S (CAS) agar. Next, 1 mL of starter cultures in 5 mL of LB medium without antibiotics incubated on a wheel rotor for 12 h at 37°C was centrifuged, and the pellet was re-suspended in sterile ice-cold PBS. Then, 5 µL were adjusted to an OD_{600} of 0.1, spotted on CAS agar plates, and incubated at 37°C for 48 h. The diameters of the colony as well as the diameter of the colony + the orange CAS halo were measured, and the CAS-reactive ring was calculated in mm according to the formula: 0.5× [(diameter of colony + CAS halo) – diameter of colony].

DNA extraction from intestinal contents

Fecal and cecal DNA were extracted using the QIAamp DNA Stool Mini Kit (Qiagen) according to the manufacturer's protocol with modifications. The protocol was extended with an initial bead-beating step using glass beads (0.5–0.75 mm) and zirconia beads (<100 µm). Lysozyme (20 mg/mL) was additionally added to the lysis buffer.

qPCR of 16S rRNA genes

16S rRNA-specific primers and hydrolysis probes were designed and validated according to the Minimum Information for Publication of Quantitative Real-Time PCR Experiments (MIQE) guidelines as detailed previously (40, 75).

qPCR reactions were performed in a LightCycler96 thermo cycler (Roche) using white LightCycler 480 Multiwell Plate 96 plates (Roche). One 20 µL reaction mixture contained 250 nM of hydrolysis probe, 300 nM of each corresponding primer, 5 ng of template genomic DNA (gDNA), water, and FastStart Essential DNA Probes Master (Roche). The sequences of primers and hydrolysis probes, the qPCR efficiencies, as well as the specificity/detection limits of qPCR assays are depicted in reference (40). All qPCR reactions were performed in duplicate applying the following conditions: 95°C for 10 min, followed by 45 cycles of 95°C for 15 s and 60°C for 1 min. Fluorescence for each cycle was recorded after the step at 60°C. Quantification cycle as well as the baseline were automatically determined by the software LightCycler 96 version 1.1 (Roche).

Animal experiments

Oligo-MM^{12} mice were generated as previously described (40) and sterilely bred in the animal housing facility of the Max von Pettenkofer-Institute. Sex- and age-matched mice were orally infected with 5×10^7 CFUs of *S*. Tm strains under germ-free conditions and maintained in gnotocages (Han, Bioscape). The protocol for neutrophil depletion was adapted from reference (36). Briefly, neutrophils were depleted by one intraperitoneal (i.p.) injection with 150 µg of α- m Ly-6G (clone: 1A8, BioXCell) prior to infection with *S*. Tm^{WT} followed by daily i.p. injections with 10 µg of α-mouse G-CSF (clone: 67604, R&D Systems). Control mice received 150 µg of Rat IgG2a (clone: 2A3, BioXCell) once and daily injections with 10 µg of Rat IgG1 (clone: 43414, R&D Systems). Antibodies were dissolved in sterile PBS. Mice were euthanized by cervical dislocation, and organs were aseptically removed. *Salmonella* loads in mesenteric lymph nodes, liver, spleen, as well as in cecal content and feces were determined by plating on MacConkey agar plates (Roth). The mouse LCN-2/NGAL detection kit (R&D Systems), ELISA kit, and horseradish peroxidase (HRP) Streptavidin (BioLegend) were used for measuring LCN-2 levels. Neutrophil-specific elastase was quantified using the Mouse Neutrophil Elastase/ELA2 DuoSet ELISA kit and the DuoSet Ancillary Reagent Kit2 (both from R&D Systems). Cecal pathology was scored at necropsy. Optimal cutting temperature compound (Sakura, Torrance) was used to embed cecal tissue. Tissues were flash frozen and cut into 5 µm cryosections. Cryosections were hematoxylin and eosin (H&E)-stained and scored as detailed in reference (76). Scoring parameters include submucosal edema, infiltration, loss of goblet cells, as well as epithelial damage. Scoring was performed in a blinded manner and yielded a total score of 0–13 points according to the severity of inflammatory symptoms (scores: 0–3: no pathological change, 4–8: mild inflammation, and 9–13: severe inflammation). All animal experiments were approved by the local authorities (Regierung von Oberbayern) and were performed according to the legal requirements.

FACS

Efficient depletion of neutrophil in the blood was monitored by FACS. Three to four drops of blood taken from the tail vein were collected in 1 mL of pre-cooled FACS buffer (PBS and 1% heat-inactivated FACS). For subsequent erythrolysis, samples were centrifuged and FACS buffer was exchanged with 1 mL of BD FACS Lysing Solution (BD). After 10 min of incubation in the dark at RT, samples were centrifuged again, Lysing Solution was discarded, and cells were resuspended in 100 µL of FACS buffer. Cells were subsequently stained with α-CD45-PerCP (clone: 30-F11, BioLegend, 1:100), α-CD11b-APC-Cy7 (clone: M1/70, BioLegend, 1:200), α-Ly-6G-Pacific Blue (clone: 1A8, BioLegend, 1:200), α-Ly-6C-FITC (clone: AL-21, BD, 1:400), α-CD3-PE (clone: 17A2, BioLegend, 1:200), and α-CD16/CD32 (93, FC-Block, eBioscience, 1:100). Following 30 min of incubation at 4°C, cells were washed and analyzed with the FACSCanto II (BD). SYTOX red (5 nM) was used to discriminate dead and living cells. Data were recorded using the BD FACSDiva software (BD) and analyzed using the FlowJo software. Neutrophils were identified as CD45$^+$, SYTOX$^-$, CD3$^-$, CD11b$^+$, Ly-6G$^+$, and Ly-6C$^{-intermediate}$ cells.

Statistical analysis

CFU data, LCN-2 levels, and pathoscores were expressed as median. More than two different groups were compared to each other using Kruskal–Wallis test, with Dunn's multiple comparison test. Two groups were compared using the Mann–Whitney U test (Prism 5; GraphPad Software, San Diego, CA, USA). The percentage of individual bacteria was expressed as mean ± SD. Differences between individual bacteria were compared using a two-way ANOVA, with Bonferroni posttest (Prism 5; GraphPad Software, San Diego, CA, USA). FACS data were expressed as the mean and analyzed using unpaired *t* test (Prism 5; GraphPad Software, San Diego, CA, USA).

To analyze clustering of qPCR data, Pearson distance matrix was used containing dissimilarity values for each pairwise comparison. Strength and statistical significance

of sample grouping were determined by applying the nonparametric Adonis method based on PERMANOVA, together with the parametric significance test PERMDISP, which analyzes multivariate homogeneity of group dispersions. The used scripts are available in QIIME (77).

In all cases, *P* values < 0.05 were considered as statistically significant.

Fold changes in absolute abundance were calculated with absolute values that were normalized to a million gene copies determined by universal probe.

ACKNOWLEDGMENTS

The work was supported by grants from the BMBF (Medizinische Infektionsgenomik), DFG Priority program SPP1656, research grants DFG STE 1971/2-1, and the German Center for Infection Research (DZIF).

M.B. and B.S. conceived and designed the study. M.B., C.E., and B.S. wrote the paper. M.B., C.E., S.H., D.R., T.D., S.B., P.S., S.H., and M.D. performed the experiments. M.B., C.E., D.G., P.M., and T.D. analyzed the data. M.B. and A.B. contributed important material. All authors approved the definitive version of the manuscript.

AUTHOR AFFILIATIONS

[1]Max von Pettenkofer Institute of Hygiene and Medical Microbiology, Faculty of Medicine, LMU Munich, Munich, Germany
[2]Computational Biology of Infection Research, Helmholtz Center for Infection Research, Braunschweig, Germany
[3]Braunschweig Integrated Center of Systems Biology (BRICS), Technische Universität Braunschweig, Braunschweig, Germany
[4]Institute of Microbiology, D-BIOL, ETH Zürich, Zürich, Switzerland
[5]Institute of Experimental Immunology, University of Zurich, Zürich, Switzerland
[6]Institute for Laboratory Animal Science and Central Animal Facility, Hannover Medical School, Hannover, Germany
[7]German Center for Infection Research (DZIF), partner site LMU Munich, Munich, Germany

AUTHOR ORCIDs

Bärbel Stecher http://orcid.org/0000-0002-7445-5193

FUNDING

Funder	Grant(s)	Author(s)
Bundesministerium für Bildung und Forschung (BMBF)	Infektionsgenomik	Bärbel Stecher
Deutsche Forschungsgemeinschaft (DFG)	SPP1656, STE 1971/2-1	Marijana Basic André Bleich Bärbel Stecher
Deutsches Zentrum für Infektionsforschung (DZIF)	TTU 06.712, TTU 06.709	Bärbel Stecher

AUTHOR CONTRIBUTIONS

Markus Beutler, Conceptualization, Investigation, Methodology, Project administration, Validation, Visualization, Writing – original draft | Claudia Eberl, Data curation, Methodology, Visualization, Writing – review and editing | Debora Garzetti, Formal analysis, Visualization | Simone Herp, Investigation | Philipp Münch, Formal analysis, Validation | Diana Ring, Formal analysis, Investigation | Tamas Dolowschiak, Formal analysis, Visualization | Sandrine Brugiroux, Investigation, Supervision | Patrick Schiller, Formal

analysis | Saib Hussain, Methodology | Marijana Basic, Investigation, Methodology | André Bleich, Supervision | Bärbel Stecher, Conceptualization, Funding acquisition, Supervision, Writing – original draft, Writing – review and editing

ADDITIONAL FILES

The following material is available online.

Supplemental Material

Supplemental figures (IAI00318-23-s0001.pdf). Fig. S1 to S8.

REFERENCES

1. GBD 2017 Disease and Injury Incidence and Prevalence Collaborators. 2018. Global, regional, and national incidence, prevalence, and years lived with disability for 354 diseases and injuries for 195 countries and territories, 1990-2017: a systematic analysis for the global burden of disease study 2017. Lancet 392:1789–1858. https://doi.org/10.1016/S0140-6736(18)32279-7
2. GBD 2017 Non-Typhoidal Salmonella Invasive Disease Collaborators. 2019. The global burden of non-typhoidal *Salmonella* invasive disease: a systematic analysis for the global burden of disease study 2017. Lancet Infect Dis 19:1312–1324. https://doi.org/10.1016/S1473-3099(19)30418-9
3. Barthel M, Hapfelmeier S, Quintanilla-Martínez L, Kremer M, Rohde M, Hogardt M, Pfeffer K, Rüssmann H, Hardt W-D. 2003. Pretreatment of mice with streptomycin provides a *Salmonella enterica* serovar Typhimurium colitis model that allows analysis of both pathogen and host. Infect Immun 71:2839–2858. https://doi.org/10.1128/IAI.71.5.2839-2858.2003
4. Wotzka SY, Kreuzer M, Maier L, Arnoldini M, Nguyen BD, Brachmann AO, Berthold DL, Zünd M, Hausmann A, Bakkeren E, et al. 2019. *Escherichia coli* limits *Salmonella* Typhimurium infections after diet shifts and fat-mediated microbiota perturbation in mice. Nat Microbiol 4:2164–2174. https://doi.org/10.1038/s41564-019-0568-5
5. Kim Y-G, Sakamoto K, Seo S-U, Pickard JM, Gillilland MG, Pudlo NA, Hoostal M, Li X, Wang TD, Feehley T, Stefka AT, Schmidt TM, Martens EC, Fukuda S, Inohara N, Nagler CR, Núñez G. 2017. Neonatal acquisition of clostridia species protects against colonization by bacterial pathogens. Science 356:315–319. https://doi.org/10.1126/science.aag2029
6. Stecher B. 2021. Establishing causality in Salmonella-microbiota-host interaction: the use of gnotobiotic mouse models and synthetic microbial communities. Int J Med Microbiol 311:151484. https://doi.org/10.1016/j.ijmm.2021.151484
7. Maier L, Vyas R, Cordova CD, Lindsay H, Schmidt TSB, Brugiroux S, Periaswamy B, Bauer R, Sturm A, Schreiber F, von Mering C, Robinson MD, Stecher B, Hardt W-D. 2013. Microbiota-derived hydrogen fuels *Salmonella* Typhimurium invasion of the gut ecosystem. Cell Host Microbe 14:641–651. https://doi.org/10.1016/j.chom.2013.11.002
8. Ng KM, Ferreyra JA, Higginbottom SK, Lynch JB, Kashyap PC, Gopinath S, Naidu N, Choudhury B, Weimer BC, Monack DM, Sonnenburg JL. 2013. Microbiota-liberated host sugars facilitate post-antibiotic expansion of enteric pathogens. Nature 502:96–99. https://doi.org/10.1038/nature12503
9. Eberl C, Weiss AS, Jochum LM, Durai Raj AC, Ring D, Hussain S, Herp S, Meng C, Kleigrewe K, Gigl M, Basic M, Stecher B. 2021. *E. coli* enhance colonization resistance against *Salmonella* Typhimurium by competing for galactitol, a context-dependent limiting carbon source. Cell Host Microbe 29:1680–1692. https://doi.org/10.1016/j.chom.2021.09.004
10. Rivera-Chávez F, Zhang LF, Faber F, Lopez CA, Byndloss MX, Olsan EE, Xu G, Velazquez EM, Lebrilla CB, Winter SE, Bäumler AJ. 2016. Depletion of butyrate-producing *Clostridia* from the gut microbiota drives an aerobic luminal expansion of *Salmonella*. Cell Host Microbe 19:443–454. https://doi.org/10.1016/j.chom.2016.03.004
11. Lopez CA, Winter SE, Rivera-Chávez F, Xavier MN, Poon V, Nuccio S-P, Tsolis RM, Bäumler AJ. 2012. Phage-mediated acquisition of a type III secreted effector protein boosts growth of *Salmonella* by nitrate respiration. mBio 3:e00143-12. https://doi.org/10.1128/mBio.00143-12
12. Nguyen BD, Cuenca VM, Hartl J, Gül E, Bauer R, Meile S, Rüthi J, Margot C, Heeb L, Besser F, Escriva PP, Fetz C, Furter M, Laganenka L, Keller P, Fuchs L, Christen M, Porwollik S, McClelland M, Vorholt JA, Sauer U, Sunagawa S, Christen B, Hardt W-D. 2020. Import of aspartate and malate by DcuABC drives H_2/fumarate respiration to promote initial *Salmonella* gut-lumen colonization in mice. Cell Host Microbe 27:922–936. https://doi.org/10.1016/j.chom.2020.04.013
13. Ackermann M, Stecher B, Freed NE, Songhet P, Hardt WD, Doebeli M. 2008. Self-destructive cooperation mediated by phenotypic noise. Nature 454:987–990. https://doi.org/10.1038/nature07067
14. Stecher B, Chaffron S, Käppeli R, Hapfelmeier S, Freedrich S, Weber TC, Kirundi J, Suar M, McCoy KD, von Mering C, Macpherson AJ, Hardt W-D. 2010. Like will to like: abundances of closely related species can predict susceptibility to intestinal colonization by pathogenic and commensal bacteria. PLoS Pathog 6:e1000711. https://doi.org/10.1371/journal.ppat.1000711
15. Stecher B, Robbiani R, Walker AW, Westendorf AM, Barthel M, Kremer M, Chaffron S, Macpherson AJ, Buer J, Parkhill J, Dougan G, von Mering C, Hardt W-D. 2007. *Salmonella enterica* serovar Typhimurium exploits inflammation to compete with the intestinal microbiota. PLoS Biol 5:2177–2189. https://doi.org/10.1371/journal.pbio.0050244
16. Barman M, Unold D, Shifley K, Amir E, Hung K, Bos N, Salzman N. 2008. Enteric salmonellosis disrupts the microbial ecology of the murine gastrointestinal tract. Infect Immun 76:907–915. https://doi.org/10.1128/IAI.01432-07
17. Stecher B, Hardt W-D. 2011. Mechanisms controlling pathogen colonization of the gut. Curr Opin Microbiol 14:82–91. https://doi.org/10.1016/j.mib.2010.10.003
18. Zhang APP, Pigli YZ, Rice PA. 2010. Structure of the LexA-DNA complex and implications for SOS box measurement. Nature 466:883–886. https://doi.org/10.1038/nature09200
19. Byndloss MX, Olsan EE, Rivera-Chávez F, Tiffany CR, Cevallos SA, Lokken KL, Torres TP, Byndloss AJ, Faber F, Gao Y, Litvak Y, Lopez CA, Xu G, Napoli E, Giulivi C, Tsolis RM, Revzin A, Lebrilla CB, Bäumler AJ. 2017. Microbiota-activated PPAR-gamma signaling inhibits dysbiotic enterobacteriaceae expansion. Science 357:570–575. https://doi.org/10.1126/science.aam9949
20. Winter SE, Thiennimitr P, Winter MG, Butler BP, Huseby DL, Crawford RW, Russell JM, Bevins CL, Adams LG, Tsolis RM, Roth JR, Bäumler AJ. 2010. Gut inflammation provides a respiratory electron acceptor for *Salmonella*. Nature 467:426–429. https://doi.org/10.1038/nature09415
21. Stecher B, Barthel M, Schlumberger MC, Haberli L, Rabsch W, Kremer M, Hardt WD. 2008. Motility allows *S.* Typhimurium to benefit from the mucosal defence. Cell Microbiol 10:1166–1180. https://doi.org/10.1111/j.1462-5822.2008.01118.x
22. Thiennimitr P, Winter SE, Winter MG, Xavier MN, Tolstikov V, Huseby DL, Sterzenbach T, Tsolis RM, Roth JR, Bäumler AJ. 2011. Intestinal inflammation allows *Salmonella* to use ethanolamine to compete with the microbiota. Proc Natl Acad Sci U S A 108:17480–17485. https://doi.org/10.1073/pnas.1107857108
23. Ali MM, Newsom DL, González JF, Sabag-Daigle A, Stahl C, Steidley B, Dubena J, Dyszel JL, Smith JN, Dieye Y, Arsenescu R, Boyaka PN, Krakowka S, Romeo T, Behrman EJ, White P, Ahmer BMM. 2014. Fructose-asparagine is a primary nutrient during growth of *Salmonella* in the inflamed intestine. PLoS Pathog 10:e1004209. https://doi.org/10.1371/journal.ppat.1004209

24. Faber F, Thiennimitr P, Spiga L, Byndloss MX, Litvak Y, Lawhon S, Andrews-Polymenis HL, Winter SE, Bäumler AJ, Sperandio V. 2017. Respiration of microbiota-derived 1,2-propanediol drives *Salmonella* expansion during colitis. PLoS Pathog 13:e1006129. https://doi.org/10.1371/journal.ppat.1006129
25. Spiga L, Winter MG, Furtado de Carvalho T, Zhu W, Hughes ER, Gillis CC, Behrendt CL, Kim J, Chessa D, Andrews-Polymenis HL, Beiting DP, Santos RL, Hooper LV, Winter SE. 2017. An oxidative central metabolism enables *Salmonella* to utilize microbiota-derived succinate. Cell Host Microbe 22:291–301. https://doi.org/10.1016/j.chom.2017.07.018
26. Gillis CC, Hughes ER, Spiga L, Winter MG, Zhu W, Furtado de Carvalho T, Chanin RB, Behrendt CL, Hooper LV, Santos RL, Winter SE. 2018. Dysbiosis-associated change in host metabolism generates lactate to support *Salmonella* growth. Cell Host Microbe 23:570. https://doi.org/10.1016/j.chom.2018.03.013
27. Raffatellu M, George MD, Akiyama Y, Hornsby MJ, Nuccio S-P, Paixao TA, Butler BP, Chu H, Santos RL, Berger T, Mak TW, Tsolis RM, Bevins CL, Solnick JV, Dandekar S, Bäumler AJ. 2009. Lipocalin-2 resistance confers an advantage to *Salmonella enterica* serotype Typhimurium for growth and survival in the inflamed intestine. Cell Host Microbe 5:476–486. https://doi.org/10.1016/j.chom.2009.03.011
28. Stecher B, Hardt WD. 2008. The role of microbiota in infectious disease. Trends Microbiol 16:107–114. https://doi.org/10.1016/j.tim.2007.12.008
29. Miki T, Goto R, Fujimoto M, Okada N, Hardt WD. 2017. The bactericidal lectin regiiibeta prolongs gut colonization and enteropathy in the streptomycin mouse model for salmonella diarrhea. Cell Host Microbe 21:195–207. https://doi.org/10.1016/j.chom.2016.12.008
30. Crawford RW, Keestra AM, Winter SE, Xavier MN, Tsolis RM, Tolstikov V, Bäumler AJ, Nassif X. 2012. Very long o-antigen chains enhance fitness during *Salmonella*-induced colitis by increasing bile resistance. PLoS Pathog 8:e1002918. https://doi.org/10.1371/journal.ppat.1002918
31. Day DW, Mandal BK, Morson BC. 1978. The rectal biopsy appearances in *Salmonella* colitis. Histopathology 2:117–131. https://doi.org/10.1111/j.1365-2559.1978.tb01700.x
32. Boyd JF. 1985. Pathology of the alimentary tract in *Salmonella* Typhimurium food poisoning. Gut 26:935–944. https://doi.org/10.1136/gut.26.9.935
33. Felmy B, Songhet P, Slack EMC, Müller AJ, Kremer M, Van Maele L, Cayet D, Heikenwalder M, Sirard J-C, Hardt W-D. 2013. NADPH oxidase deficient mice develop colitis and bacteremia upon infection with normally avirulent, TTSS-1- and TTSS-2-deficient *Salmonella* Typhimurium. PLoS One 8:e77204. https://doi.org/10.1371/journal.pone.0077204
34. Loetscher Y, Wieser A, Lengefeld J, Kaiser P, Schubert S, Heikenwalder M, Hardt W-D, Stecher B. 2012. *Salmonella* transiently reside in luminal neutrophils in the inflamed gut. PLoS One 7:e34812. https://doi.org/10.1371/journal.pone.0034812
35. Molloy MJ, Grainger JR, Bouladoux N, Hand TW, Koo LY, Naik S, Quinones M, Dzutsev AK, Gao J-L, Trinchieri G, Murphy PM, Belkaid Y. 2013. Intraluminal containment of commensal outgrowth in the gut during infection-induced dysbiosis. Cell Host & Microbe 14:318–328. https://doi.org/10.1016/j.chom.2013.08.003
36. Maier L, Diard M, Sellin ME, Chouffane E-S, Trautwein-Weidner K, Periaswamy B, Slack E, Dolowschiak T, Stecher B, Loverdo C, Regoes RR, Hardt W-D. 2014. Granulocytes impose a tight bottleneck upon the gut luminal pathogen population during *Salmonella* Typhimurium colitis. PLoS Pathog 10:e1004557. https://doi.org/10.1371/journal.ppat.1004557
37. Gill N, Ferreira RBR, Antunes LCM, Willing BP, Sekirov I, Al-Zahrani F, Hartmann M, Finlay BB. 2012. Neutrophil elastase alters the murine gut microbiota resulting in enhanced *Salmonella* colonization. PLoS One 7:e49646. https://doi.org/10.1371/journal.pone.0049646
38. Liu JZ, Jellbauer S, Poe AJ, Ton V, Pesciaroli M, Kehl-Fie TE, Restrepo NA, Hosking MP, Edwards RA, Battistoni A, Pasquali P, Lane TE, Chazin WJ, Vogl T, Roth J, Skaar EP, Raffatellu M. 2012. Zinc sequestration by the neutrophil protein calprotectin enhances *Salmonella* growth in the inflamed gut. Cell Host Microbe 11:227–239. https://doi.org/10.1016/j.chom.2012.01.017
39. Lawley TD, Bouley DM, Hoy YE, Gerke C, Relman DA, Monack DM. 2008. Host transmission of *Salmonella enterica* serovar Typhimurium is controlled by virulence factors and indigenous intestinal Microbiota. Infect Immun 76:403–416. https://doi.org/10.1128/IAI.01189-07
40. Brugiroux S, Beutler M, Pfann C, Garzetti D, Ruscheweyh H-J, Ring D, Diehl M, Herp S, Lötscher Y, Hussain S, Bunk B, Pukall R, Huson DH, Münch PC, McHardy AC, McCoy KD, Macpherson AJ, Loy A, Clavel T, Berry D, Stecher B. 2016. Genome-guided design of a defined mouse microbiota that confers colonization resistance against *Salmonella enterica* serovar Typhimurium. Nat Microbiol 2:16215. https://doi.org/10.1038/nmicrobiol.2016.215
41. Weiss AS, Burrichter AG, Durai Raj AC, von Strempel A, Meng C, Kleigrewe K, Münch PC, Rössler L, Huber C, Eisenreich W, Jochum LM, Göing S, Jung K, Lincetto C, Hübner J, Marinos G, Zimmermann J, Kaleta C, Sanchez A, Stecher B. 2022. *In vitro* interaction network of a synthetic gut bacterial community. ISME J 16:1095–1109. https://doi.org/10.1038/s41396-021-01153-z
42. Weiss AS, Niedermeier LS, von Strempel A, Burrichter AG, Ring D, Meng C, Kleigrewe K, Lincetto C, Hübner J, Stecher B. 2023. Nutritional and host environments determine community ecology and keystone species in a synthetic gut bacterial community. Nat Commun 14:4780. https://doi.org/10.1038/s41467-023-40372-0
43. Hoces D, Lan J, Sun W, Geiser T, Stäubli ML, Cappio Barazzone E, Arnoldini M, Challa TD, Klug M, Kellenberger A, Nowok S, Faccin E, Macpherson AJ, Stecher B, Sunagawa S, Zenobi R, Hardt W-D, Wolfrum C, Slack E. 2022. Metabolic reconstitution of germ-free mice by a gnotobiotic Microbiota varies over the circadian cycle. PLoS Biol 20:e3001743. https://doi.org/10.1371/journal.pbio.3001743
44. Afrizal A, Jennings SAV, Hitch TCA, Riedel T, Basic M, Panyot A, Treichel N, Hager FT, Wong E-Y, Wolter B, et al. 2022. Enhanced cultured diversity of the mouse gut microbiota enables custom-made synthetic communities. Cell Host Microbe 30:1630–1645. https://doi.org/10.1016/j.chom.2022.09.011
45. Osbelt L, Wende M, Almási É, Derksen E, Muthukumarasamy U, Lesker TR, Galvez EJC, Pils MC, Schalk E, Chhatwal P, Färber J, Neumann-Schaal M, Fischer T, Schlüter D, Strowig T. 2021. *Klebsiella oxytoca* causes colonization resistance against multidrug-resistant *K. pneumoniae* in the gut via cooperative carbohydrate competition. Cell Host Microbe 29:1663–1679. https://doi.org/10.1016/j.chom.2021.09.003
46. Studer N, Desharnais L, Beutler M, Brugiroux S, Terrazos MA, Menin L, Schürch CM, McCoy KD, Kuehne SA, Minton NP, Stecher B, Bernier-Latmani R, Hapfelmeier S. 2016. Functional intestinal bile acid 7α-dehydroxylation by *Clostridium scindens* associated with protection from *Clostridium difficile* infection in a gnotobiotic mouse model. Front Cell Infect Microbiol 6:191. https://doi.org/10.3389/fcimb.2016.00191
47. van Tilburg Bernardes E, Pettersen VK, Gutierrez MW, Laforest-Lapointe I, Jendzjowsky NG, Cavin J-B, Vicentini FA, Keenan CM, Ramay HR, Samara J, MacNaughton WK, Wilson RJA, Kelly MM, McCoy KD, Sharkey KA, Arrieta M-C. 2020. Intestinal fungi are causally implicated in microbiome assembly and immune development in mice. Nat Commun 11:2577. https://doi.org/10.1038/s41467-020-16431-1
48. Lourenço M, Chaffringeon L, Lamy-Besnier Q, Pédron T, Campagne P, Eberl C, Bérard M, Stecher B, Debarbieux L, De Sordi L. 2020. The spatial heterogeneity of the gut limits predation and fosters coexistence of bacteria and bacteriophages. Cell Host Microbe 28:390–401. https://doi.org/10.1016/j.chom.2020.06.002
49. Ye H, Borusak S, Eberl C, Krasenbrink J, Weiss AS, Chen S-C, Hanson BT, Hausmann B, Herbold CW, Pristner M, Zwirzitz B, Warth B, Pjevac P, Schleheck D, Stecher B, Loy A. 2023. Ecophysiology and interactions of a taurine-respiring bacterium in the mouse gut. Nat Commun 14:5533. https://doi.org/10.1038/s41467-023-41008-z
50. Miller BM, Bäumler AJ. 2021. The habitat filters of microbiota-nourishing immunity. Annu Rev Immunol 39:1–18. https://doi.org/10.1146/annurev-immunol-101819-024945
51. Stecher B, Maier L, Hardt WD. 2013. Blooming' in the gut: how dysbiosis might contribute to pathogen evolution. Nat Rev Microbiol 11:277–284. https://doi.org/10.1038/nrmicro2989
52. Stecher B, Denzler R, Maier L, Bernet F, Sanders MJ, Pickard DJ, Barthel M, Westendorf AM, Krogfelt KA, Walker AW, Ackermann M, Dobrindt U, Thomson NR, Hardt WD. 2012. Gut inflammation can boost horizontal gene transfer between pathogenic and commensal enterobacteriaceae. Proc Natl Acad Sci U S A 109:1269–1274. https://doi.org/10.1073/pnas.1113246109
53. Diard M, Bakkeren E, Cornuault JK, Moor K, Hausmann A, Sellin ME, Loverdo C, Aertsen A, Ackermann M, De Paepe M, Slack E, Hardt W-D.

2017. Inflammation boosts bacteriophage transfer between *Salmonella* spp. Science 355:1211–1215. https://doi.org/10.1126/science.aaf8451
54. Wotzka SY, Nguyen BD, Hardt WD. 2017. *Salmonella* Typhimurium diarrhea reveals basic principles of enteropathogen infection and disease-promoted DNA exchange. Cell Host Microbe 21:443–454. https://doi.org/10.1016/j.chom.2017.03.009
55. Lamy-Besnier Q, Chaffringeon L, Lourenço M, Payne RB, Trinh JT, Schwartz JA, Sulakvelidze A, Debarbieux L. 2021. Prophylactic administration of a bacteriophage cocktail is safe and effective in reducing *Salmonella enterica* serovar Typhimurium burden *in vivo*. Microbiol Spectr 9:e0049721. https://doi.org/10.1128/spectrum.00497-21
56. Weiss AS, Burrichter AG, Durai Raj AC, von Strempel A, Meng C, Kleigrewe K, Münch PC, Rössler L, Huber C, Eisenreich W, Jochum LM, Göing S, Jung K, Lincetto C, Hübner J, Marinos G, Zimmermann J, Kaleta C, Sanchez A, Stecher B. 2022. *In vitro* interaction network of a synthetic gut bacterial community. ISME J 16:1095–1109. https://doi.org/10.1038/s41396-021-01153-z
57. Rhee SJ, Walker WA, Cherayil BJ. 2005. Developmentally regulated intestinal expression of IFN-gamma and its target genes and the age-specific response to enteric *Salmonella* infection. J Immunol 175:1127–1136. https://doi.org/10.4049/jimmunol.175.2.1127
58. Godinez I, Haneda T, Raffatellu M, George MD, Paixão TA, Rolán HG, Santos RL, Dandekar S, Tsolis RM, Bäumler AJ. 2008. T cells help to amplify inflammatory responses induced by *Salmonella enterica* serotype Typhimurium in the intestinal mucosa. Infect Immun 76:2008–2017. https://doi.org/10.1128/IAI.01691-07
59. Knodler LA, Vallance BA, Celli J, Winfree S, Hansen B, Montero M, Steele-Mortimer O. 2010. Dissemination of invasive *Salmonella* via bacterial-induced extrusion of mucosal epithelia. Proc Natl Acad Sci U S A 107:17733–17738. https://doi.org/10.1073/pnas.1006098107
60. Sellin ME, Müller AA, Felmy B, Dolowschiak T, Diard M, Tardivel A, Maslowski KM, Hardt W-D. 2014. Epithelium-intrinsic NAIP/Nlrc4 Inflammasome drives infected enterocyte expulsion to restrict *Salmonella* replication in the intestinal mucosa. Cell Host Microbe 16:237–248. https://doi.org/10.1016/j.chom.2014.07.001
61. Songhet P, Barthel M, Stecher B, Müller AJ, Kremer M, Hansson GC, Hardt W-D, Bereswill S. 2011. Stromal IFN-γR-signaling modulates goblet cell function during *Salmonella* Typhimurium infection. PLoS ONE 6:e22459. https://doi.org/10.1371/journal.pone.0022459
62. Hapfelmeier S, Stecher B, Barthel M, Kremer M, Müller AJ, Heikenwalder M, Stallmach T, Hensel M, Pfeffer K, Akira S, Hardt W-D. 2005. The *Salmonella* pathogenicity island (SPI)-1 and SPI-2 type III secretion systems allow *Salmonella* serovar Typhimurium to trigger colitis via myd88-dependent and myd88-independent mechanisms. J Immunol 174:1675–1685. https://doi.org/10.4049/jimmunol.174.3.1675
63. Thiennimitr P, Winter SE, Bäumler AJ. 2012. *Salmonella*, the host and its Microbiota. Curr Opin Microbiol 15:108–114. https://doi.org/10.1016/j.mib.2011.10.002
64. Cheng AG, Ho P-Y, Aranda-Díaz A, Jain S, Yu FB, Meng X, Wang M, Iakiviak M, Nagashima K, Zhao A, Murugkar P, Patil A, Atabakhsh K, Weakley A, Yan J, Brumbaugh AR, Higginbottom S, Dimas A, Shiver AL, Deutschbauer A, Neff N, Sonnenburg JL, Huang KC, Fischbach MA. 2022. Design, construction, and *in vivo* augmentation of a complex gut microbiome. Cell 185:3617–3636. https://doi.org/10.1016/j.cell.2022.08.003
65. Clavel T, Lagkouvardos I, Blaut M, Stecher B. 2016. The mouse gut microbiome revisited: from complex diversity to model ecosystems. Int J Med Microbiol 306:316–327. https://doi.org/10.1016/j.ijmm.2016.03.002
66. Hoiseth SK, Stocker BA. 1981. Aromatic-dependent *Salmonella* Typhimurium are non-virulent and effective as live vaccines. Nature 291:238–239. https://doi.org/10.1038/291238a0
67. Ehrbar K, Hapfelmeier S, Stecher B, Hardt WD. 2004. InvB is required for type III-dependent secretion of SopA in *Salmonella enterica* serovar Typhimurium. J Bacteriol 186:1215–1219. https://doi.org/10.1128/JB.186.4.1215-1219.2004
68. Kaniga K, Bossio JC, Galán JE. 1994. The *Salmonella* Typhimurium invasion genes invF and invG encode homologues of the AraC and PulD family of proteins. Mol Microbiol 13:555–568. https://doi.org/10.1111/j.1365-2958.1994.tb00450.x
69. Datsenko KA, Wanner BL. 2000. One-step inactivation of chromosomal genes in *Escherichia col*i K-12 using PCR products. Proc Natl Acad Sci U S A 97:6640–6645. https://doi.org/10.1073/pnas.120163297
70. Schmieger H. 1972. Phage P22-mutants with increased or decreased transduction abilities. Mol Gen Genet 119:75–88. https://doi.org/10.1007/BF00270447
71. Deiwick J, Hensel M. 1999. Regulation of virulence genes by environmental signals in Salmonella Typhimurium. Electrophoresis 20:813–817. https://doi.org/10.1002/(SICI)1522-2683(19990101)20:4/5<813::AID-ELPS813>3.0.CO;2-Q
72. Cherepanov PP, Wackernagel W. 1995. Gene disruption in *Escherichia coli*: TcR and KmR cassettes with the option of Flp-catalyzed excision of the antibiotic-resistance determinant. Gene 158:9–14. https://doi.org/10.1016/0378-1119(95)00193-a
73. Miranda KM, Espey MG, Wink DA. 2001. A rapid, simple spectrophotometric method for simultaneous detection of nitrate and nitrite. Nitric Oxide 5:62–71. https://doi.org/10.1006/niox.2000.0319
74. Bapteste E, Bicep C, Lopez P. 2012. Evolution of genetic diversity using networks: the human gut Microbiome as a case study. Clin Microbiol Infect 18:40–43. https://doi.org/10.1111/j.1469-0691.2012.03856.x
75. Bustin SA, Benes V, Garson JA, Hellemans J, Huggett J, Kubista M, Mueller R, Nolan T, Pfaffl MW, Shipley GL, Vandesompele J, Wittwer CT. 2009. The MIQE guidelines: minimum information for publication of quantitative real-time PCR experiments. Clin Chem 55:611–622. https://doi.org/10.1373/clinchem.2008.112797
76. Gerlach RG, Jäckel D, Stecher B, Wagner C, Lupas A, Hardt W-D, Hensel M. 2007. *Salmonella* pathogenicity island 4 encodes a giant non-fimbrial adhesin and the cognate type 1 secretion system. Cell Microbiol 9:1834–1850. https://doi.org/10.1111/j.1462-5822.2007.00919.x
77. Caporaso JG, Kuczynski J, Stombaugh J, Bittinger K, Bushman FD, Costello EK, Fierer N, Peña AG, Goodrich JK, Gordon JI, et al. 2010. QIIME allows analysis of high-throughput community sequencing data. Nat Methods 7:335–336. https://doi.org/10.1038/nmeth.f.303